Chemical Engineering Journal 522 (2025) 167120

Contents lists available at ScienceDirect

Chemical Engineering Journal

journal homepage: www.elsevier.com/locate/cej

Hierarchically shortened *b*-axis ZSM-5 nanosheet endows super catalytic stability for methanol-to-hydrocarbons reaction

Zhan Liu [a,b,1], Ying-Jun He [c,1], Zhi-Yi Hu [a,b,*], Jia-Min Lyu [a], Shen Yu [a], Yu-Hang Song [a], Xiao-Qiang Liao [a,b], Zhi-Wen Yin [a,b], Ming-Hui Sun [a], Yu-Chun Zhi [c], Li-Hua Chen [a,**], Bao-Lian Su [a,d,*]

[a] *State Key Laboratory of Advanced Technology for Materials Synthesis and Processing, Wuhan University of Technology, 122 Luoshi Road, 430070 Wuhan, Hubei, China*

[b] *NRC (Nanostructure Research Centre), Wuhan University of Technology, 122 Luoshi Road, 430070 Wuhan, Hubei, China*

[c] *National Engineering Laboratory for Methanol to Olefins, State Energy Low Carbon Catalysis and Engineering R&D Center, Dalian National Laboratory for Clean Energy, iChEM (Collaborative Innovation Center of Chemistry for Energy Materials), Dalian Institute of Chemical Physics, Chinese Academy of Sciences, Dalian 116023, China*

[d] *CMI (Laboratory of Inorganic Materials Chemistry), University of Namur, 61 rue de Bruxelles, B-5000 Namur, Belgium*

ARTICLE INFO

Keywords:
Methanol-to-hydrocarbons
ZSM-5 nanosheet
Hierarchical pore
Shortened *b*-axis straight channel
Chemical etching

ABSTRACT

The design of hierarchically porous zeolites with ultra-thin *b*-axis thickness is regarded as an effective strategy to improve the diffusion efficiency, product selectivity and catalytic lifetime of the methanol-to-hydrocarbons (MTH) reaction. However, it is still a great challenge to simultaneously obtain interconnected hierarchical single crystal zeolites and the thin shortened *b*-axis structure. Herein, we constructed an hourglass-shaped-hollow hierarchical structure into the shortened *b*-axis zeolite ZSM-5 single crystal through chemical etching strategy, and its shortest diffusion length along *b*-axis direction is less than 30 nm. The silicon-rich composition and high defects density inside the zeolite together with the protective effect of urea and TPA^+ organic residues on the outer surface make the central area and the connected side symmetrical volume pair composed of {101} and {10–1} facets are preferentially etched. Such hierarchically porous ZSM-5 nanosheet catalysts displayed a greatly prolonged MTH catalytic lifetime (63.1 h) which was 5 times longer than that of the microsized ZSM-5 zeolite (12.7 h) due to the enhanced diffusivity, anti-coke ability and increased micropore accessibility. This work provides a facile and controllable strategy to prepare hierarchical shortened *b*-axis MFI-type single crystal zeolite for highly stable MTH reaction, and deep understand on the formation mechanism of etching method in the zeolite synthetic system.

1. Introduction

The methanol-to-hydrocarbons (MTH) conversion is one of the most important chemical reaction without relying on oil resources in heterogeneous catalysis [1–5], which can convert abundant coal, natural gas and biomass into important chemicals and fuels such as low-carbon olefins (MTO) [6–8], aromatic hydrocarbons (MTA) [9–11] and gasoline (MTG) [12–14]. ZSM-5 zeolite exhibits superior catalytic performance in the MTH reaction, because of its unique acid active center and shape selectivity of ordered MFI-type topology [15–17]. However, the small micropores (< 2 nm) with the long channel length (especially the straight channel along *b*-axis direction) of ZSM-5 zeolite results in the severe diffusion limitation, thus leading to the undesirable coke formation and rapid deactivation [18–20]. Therefore, it is important to find an economical and facile approach to enhance the diffusion efficiency of the catalysts, so as to improve the specific product selectivity or/and catalytic lifetime of the MTH process.

One of the most effective strategies to improve the diffusivity of MFI-

* Corresponding authors at: State Key Laboratory of Advanced Technology for Materials Synthesis and Processing, Wuhan University of Technology, 122 Luoshi Road, 430070 Wuhan, Hubei, China.
** Corresponding author.
E-mail addresses: zhiyi.hu@whut.edu.cn (Z.-Y. Hu), chenlihua@whut.edu.cn (L.-H. Chen), bao-lian.su@unamur.be (B.-L. Su).
[1] These authors contributed equally.

https://doi.org/10.1016/j.cej.2025.167120
Received 3 January 2025; Received in revised form 14 July 2025; Accepted 10 August 2025
Available online 14 August 2025

type zeolites is to shorten the *b*-axis thickness, because the shortened straight channel along the [010] direction can greatly improve the intragranular diffusion process of guest molecules [21–23]. Especially when the *b*-axis thickness becomes less than 50 nm, the impact of diffusion limitations is substantially alleviated [24,25]. Meanwhile, the introduction of hierarchically porous structure can also effectively improve the zeolite diffusivity as well as the MTH catalytic ability, due to the combination of the intrinsic acid active sites in micropores and the enhanced diffusivity of the additional meso-/macroporous system [26–30]. Hence, it is of great significance to develop synthetic strategies to simultaneously construct the hierarchical structure and zeolite materials of shortened *b*-axis length. In this case, Choi *et al.* synthesized polycrystalline hierarchical MFI zeolite assembled by ultrathin nanosheets via employing a di-quaternary ammonium bifunctional surfactant [31]. Further, the anisotropic etching method provides a more facile strategy to obtain shortened *b*-axis hierarchical zeolite single crystals from related microcrystals [32–34]. For example, Zhou and Liu *et al.* successfully prepared ZSM-5 zeolites with uniform nanosheet morphology and interconnected mesoporosity via simple alkaline etching [35,36]. However, it is still a challenge to synthesize hierarchically shortened *b*-axis MFI nanosheets with diffusion length less than 50 nm, simultaneously exhibit high crystallinity and super stability.

Herein, an hourglass-shaped-hollow hierarchical zeolite ZSM-5 nanosheet with the shortest diffusion length along *b*-axis direction less than 30 nm has been constructed successfully by the etching strategy. The hourglass-shaped area is rich in silicon and high in defect density, so the etching molecules rapidly diffuse into the ZSM-5 crystal from abundant *b*-axis straight channel openings and preferentially etch the region. Such innovative hourglass-shaped-hollow structure endows an excellent MTH catalytic performance, and its catalytic lifetime (63.1 h, WHSV = 5 h^{-1}, T = 480 °C, methanol conversion > 95 %) was 5 times longer than that of the microsized ZSM-5 zeolite (12.7 h) with a similar Si/Al ratio. This work provides a strategy for the facile and controllable preparation of hierarchical single-crystal MFI-type zeolite with enhanced straight channel diffusion ability.

2. Experimental sections and characterizations

2.1. Hourglass-shaped-hollow hierarchical ZSM-5 single crystal preparation

2.1.1. Synthesis of shortened b-axis platelike ZSM-5 zeolites

Typically, 0.08 g aluminum isopropoxide (AIP) and 0.9 g urea were added into the mixture of 3.6 g tetrapropylammonium hydroxide (TPAOH, 2.0 M in H_2O) and 10.8 g H_2O. And then added 8.3 g tetraethyl orthosilicate (TEOS) after AIP and urea were completely dissolved. The mixture was stirred continuously for 4 h until clarification. Afterwards, the obtained solution was transferred into a 150 mL Teflon-lined stainless-steel autoclave and hydrothermal crystallized at 180 °C for 24 h. The obtained product was washed with deionized water by filtration, dried at 60 °C in the oven overnight, and finally calcinated at 550 °C for 7 h with a rate of 2 °C min^{-1}.

2.1.2. Synthesis of hourglass-shaped-hollow hierarchically macro-/meso-/microporous ZSM-5 zeolite single crystals

Briefly, 0.5 g platelike ZSM-5 zeolite prepared above was added into 25 mL of 0.2 M NaOH solution, and stirred at 80 °C for 15 min in an oil bath pot. The etched product was washed with abundant deionized water several times by filtration, dried at 60 °C for several hours, and then calcinated in a muffle furnace at 550 °C for 7 h. In addition, the H-type ZSM-5 zeolites with shortened *b*-axis thickness were prepared via an ion-exchange process. The 0.5 g as-prepared ZSM-5 zeolites were dispersed in 12.5 mL of 1.0 M NH_4NO_3 solution at 80 °C for 3 h. Afterwards, the product was washed with deionized water and calcinated at 550 °C for 7 h. The above ammonia exchange process was repeated for three times.

2.2. Nanosized and microsized ZSM-5 zeolite preparation

The nanosized ZSM-5 zeolite was synthesized by the following method. 0.04 g AIP was added into the mixture of 1.8 g TPAOH (2.0 M in H_2O) and 5.4 g water, stirred for 1 h, then added 4.2 g TEOS. The solution was stirred continuously for 4 h. Afterwards, the obtained clear solution was transferred into an autoclave and crystallized at 180 °C for 24 h. The product was washed with deionized water, dried at 60 °C overnight, and calcinated in a muffle furnace at 550 °C for 7 h.

The microsized ZSM-5 zeolite was prepared by the following method. Mixed 2.0 g TPAOH (25 wt%), 20.0 g water, 0.04 g sodium aluminate and 10.4 g TEOS together, and stirred for 5 h. The obtained gel was then transferred into an autoclave and crystallized at 180 °C for 24 h. The product was washed with abundant water, dried at 60 °C overnight, and calcinated at 550 °C for 7 h.

2.3. Material characterizations

The scanning electron microscopy (SEM) images were collected on a Hitachi S-4800 field-emission SEM with 5.0 kV extraction voltage and 10.0 μA acceleration current. The transmission electron microscopy (TEM), high-resolution transmission electron microscopy (HR-TEM), high-angle annular dark-fields scanning transmission electron microscopy (HAADF-STEM) and selected area electron diffraction (SAED) studies were performed on a Thermo Fisher Themis microscope fitted with aberration correctors for both the probe forming and the imaging lens, which operated at 300 kV with atomic resolution. The elemental mapping results were acquired by the scanning transmission electron microscopy (STEM) mode in the combination with energy dispersive X-ray spectroscopy (EDX) analysis. Three-dimensional (3D) electron tomographic reconstruction and corresponding HAADF-STEM orthoslices were performed through Inspect 3D software using SIRT model visualized by Avizo.

The X-ray diffraction (XRD) patterns were recorded on a D8 ADVANCE with Cu Kα radiation (λ = 1.5413 Å). The measurements were taken at a tube voltage of 40 kV and a tube current of 40 mA under ambient conditions. All the data were collected in the range of 2θ from 5° to 40° with a step increase of 0.05° min^{-1}. The Fourier Transform Infrared Spectrometer (FTIR) spectra in the OH stretching region were obtained on a Bruker INVENIO-S equipped with a MCT detector and a Harrick diffuse reflection *in-situ* bin. The samples were pretreated at 450 °C for 4 h with 10^{-4} vacuum degree, and the spectra were recorded in He at 200 °C. The ^{27}Al and ^{29}Si solid-state nuclear magnetic resonance (NMR) spectra were measured on a Varian VNMRS spectrometer with a 9.4 T (^{27}Al freq. = 79.46 MHz; ^{29}Si freq. = 79.46 MHz) using a Varian/Chemagnetics HX 4 mm CP/MAS probe. The samples were packed in a standard 4 mm rotor and spun at 10 kHz. The number of transient ranges between ~200 and 11000 for the ^{29}Si spectra, and between 2000 and 3500 for the ^{27}Al spectra.

The nitrogen adsorption-desorption isotherms were recorded by using a Micromeritics ASAP 2460 Version 3.01 gas sorptiometer after the samples were degassed at 300 °C under vacuum for 12 h. The micropore surface areas and volumes were determined from N_2 adsorption using t-plot method, and the micropore size distributions were derived from the adsorption branches of N_2 isotherms with relative pressure P/P_0 of < 0.01 calculated by using the Horvath-Kawazoe (HK) model. The BET surface areas and the mesopore size distributions were determined by the desorption branches of N_2 isotherms calculated by using the Barrett-Joyner-Halenda (BJH) model. The total pore volumes were estimated from single point N_2 adsorption amount at a relative pressure P/P_0 = 0.99. The mercury intrusion porosimetry (MIP) measurements were measured with a Micromeritics Autopore IV 9500 operated in the pressure range from vacuum to 207 MPa. The macropore size distribution was determined by the application of the Washburn equation.

The ammonia temperature-programmed desorption (NH_3-TPD) tests

were measured on Micromeritics Auto Chem II 2920 chemisorption apparatus. The infrared spectroscopy of pyridine adsorption (Py-IR) measurements used pyridine as a probe molecule on a Bruker Tensor 27 Fourier Transform Infrared spectrometer (FTIR), and the spectra were obtained in the 1400–1700 cm^{-1} at different temperatures (200 °C, 350 °C, and 450 °C). The chemical composition of the samples was determined by inductively coupled plasma-optical emission spectroscopy (ICP-OES) using Agilent 5110 (OES).

2.4. Catalytic test

100 mg catalyst was pressed, sieved to 40–60 mesh and loaded in a fixed-bed quartz tubular reactor with inner diameter of 4 mm. Prior to the reaction, the catalyst was activated at 500 °C for 40 min, and then the temperature was adjusted to 480 °C. Methanol was fed by passing the N_2 carrier gas through a saturator containing methanol. By changing the volumetric flow rate of N_2 and the temperature of saturator, varying molar fraction and weight hourly space velocity (WHSV) of methanol can be acquired. Methanol conversion was performed under atmospheric pressure. The effluent products from reactor were kept warm and analyzed by online gas chromatography equipped with a PoraPLOT Q-HT capillary column and an FID detector. The conversion and selectivity were calculated on CH_2 basis. Dimethyl ether (DME) was considered as reactant in the calculation. Conversion and selectivity were calculated as follows:

$$\text{Conversion} = \left[1 - \left(\frac{C_{MeOH} + C_{DME} \times 2}{C_{C1} + C_{C2} \times 2 + C_{C3} \times 3 + \ldots}\right)\right] \times 100\% \quad (1)$$

$$\text{Selectivity} = \frac{C_{C1\ product}/C_{C2\ product} \times 2/C_{C3\ product} \times 3/\ldots}{C_{C1\ product} + C_{C2\ product} \times 2 + C_{C3\ product} \times 3 + \ldots} \times 100\% \quad (2)$$

C_{MeOH}, C_{DME}, C_{C1}, C_{C2}, C_{C3}, $C_{C1\ product}$, $C_{C2\ product}$ and $C_{C3\ product}$ represent the concentration of methanol (MeOH), dimethyl ether (DME), C1 species, C2 species, C3 species, C1 products, C2 products and C3 products, respectively. Particularly, $C_{C1\ product}$ includes the concentration of CO and CO_2, C_{C1} includes $C_{C1\ product}$ and the concentration of MeOH, and C_{C2} includes $C_{C2\ product}$ and the concentration of DME. The concentration of each substance is calculated by the corresponding standard gas with known concentration by external standard method.

3. Results and discussion

Typically, the hierarchically interconnected zeolite ZSM-5 nanosheet with a unique hourglass-shaped-hollow structure (Figs. 1a and S2) was

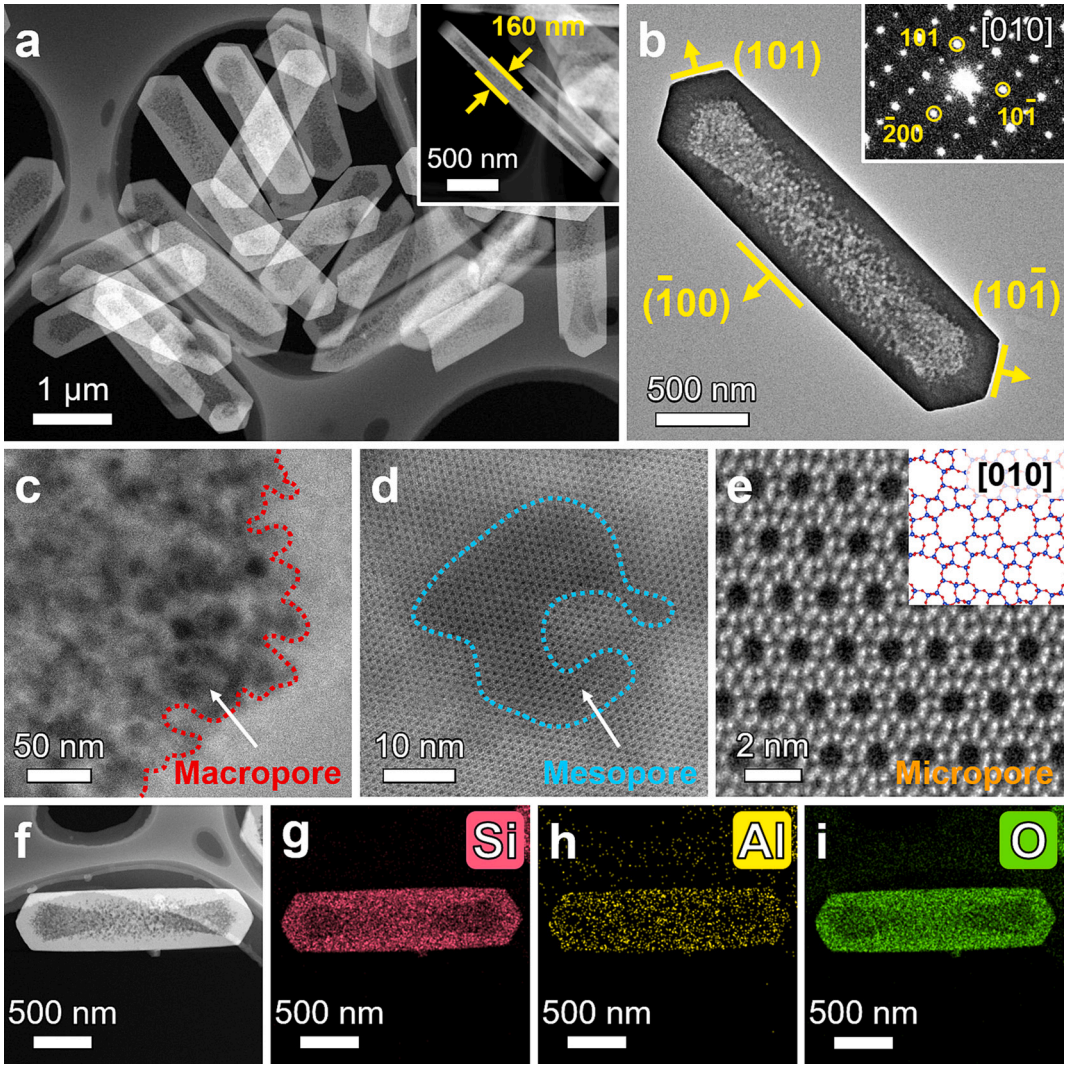

Fig. 1. (a) HAADF-STEM images of hourglass-shaped-hollow hierarchical ZSM-5 zeolites. (b) TEM image and the corresponding (b inset) SAED pattern of an individual hourglass-shaped-hollow hierarchical ZSM-5 single crystal. (c–e) HAADF-STEM images of (c) macropores, (d) mesopores and (e) micropores of the hourglass-shaped-hollow hierarchical ZSM-5 single crystal. (f) HAADF-STEM image and the corresponding (g–i) EDX mappings of Si, Al and O elements of one hourglass-shaped-hollow hierarchical ZSM-5 single crystal.

synthesized from the platelike ZSM-5 zeolite with a 160 nm shortened *b*-axis (Fig. S1) through the alkaline desilication strategy. The transmission electron microscopy (TEM) image (Fig. 1b) shows the typical structure of one hourglass-shaped-hollow hierarchical ZSM-5 nanosheet in detail, in which the central region and the connected side symmetrical volume pair composed of {101} and {10–1} facets were seriously etched. The selected area electron diffraction (SAED) pattern exhibits a typical single crystal characteristic along the MFI-type [010] orientation (Fig. 1b inset). The high-angle annular dark-fields scanning transmission electron microscopy (HAADF-STEM) images in Fig. 1c–e display the abundant macro-/meso-/micropores of the obtained hierarchical zeolite. Particularly, the small macropores and mesopores etched in the nanosheet are highly interconnected with the overall hourglass-shaped macropores (Fig. 1c, d), which are all surrounded by typical MFI topological micropores visualized by Fig. 1e. Such hierarchically hourglass-shaped-hollow structure is expected to perform an excellent pore-to-pore connectivity and remarkable active sites accessibility. In addition, the energy dispersive X-ray spectroscopy (EDX) mappings indicate that the Si, Al and O elements are homogeneously distributed (Fig. 1f–i). Compared with Al element, the distribution of Si and O has a more obvious hourglass-shaped morphology affected by NaOH desilicated.

The 3D electron tomographic reconstruction result exhibits the overall morphology of one hierarchically hourglass-shaped-hollow zeolite ZSM-5 nanosheet (Fig. 2a), which shows a significantly prolonged *c*-axis including abundant shortened *b*-axis straight channel openings. The 3D reconstruction orthoslices along the *b*-axis (Fig. 2b), *a*-axis (Fig. 2c, e) and *c*-axis (Fig. 2d, f) reveal that the macropores and mesopores mainly extend in the direction parallel to the *b*-axis, while the outer surface is hardly etched. Noted that the thickness of the outer shell on (010) surface is less than 30 nm, which can substantially shorten the diffusion path and alleviate the impact of diffusion limitations [24]. The continuous orthoslices along the above three main crystal directions shown in Figs. S3–S5 further clearly demonstrates the abundant and interconnected meso-/macroporous structure of the obtained hourglass-shaped-hollow ZSM-5 single crystal. Based on the above characterization, the model schematic illustration of the hourglass-shaped-hollow hierarchically porous ZSM-5 zeolite has been designed to finely reduce the spatial structure of the crystal (Fig. 2g), in which the deep orange parts (a_1 and a_1', a_2 and a_2', and a_3 and a_3') represent the weak etched regions, while the light orange parts (b_1, b_1' and c) represent the hourglass-shaped strong etched regions. Therefore, the hierarchically shortened *b*-axis ZSM-5 nanosheets with interconnected hourglass-shaped-hollow macro-/meso-/microporous structure have been successfully synthesized.

Furthermore, the etching process of NaOH desilication is illustrated by Figs. 3a and S6. The samples treated with NaOH for 0, 5, 10, 15, 20 and 25 min are named as AT-0, AT-5, AT-10, AT-15, AT-20 and AT-25, respectively. In the initial stage of NaOH desilication, the internal region of the ZSM-5 zeolite with complete platelike crystal structure (Figs. 3b, h and S7) is uniformly etched to form an obvious point-like porous structure (Figs. 3c, i and S8). Subsequently, as the etching degree inside the zeolite increased in several areas, a regional irregular macroporous structure was formed (Figs. 3d, j and S9). And a typical hourglass-shaped-hollow hierarchical structure can be successfully formed after desilication for 15 min (Fig. 3e, k). It is worth noting that the hourglass-shaped etching structure probably reflects the intrinsic growth process of the platelike ZSM-5 zeolite. That is, the zeolites preferentially grow into a silicon-rich central core and the connected side symmetrical

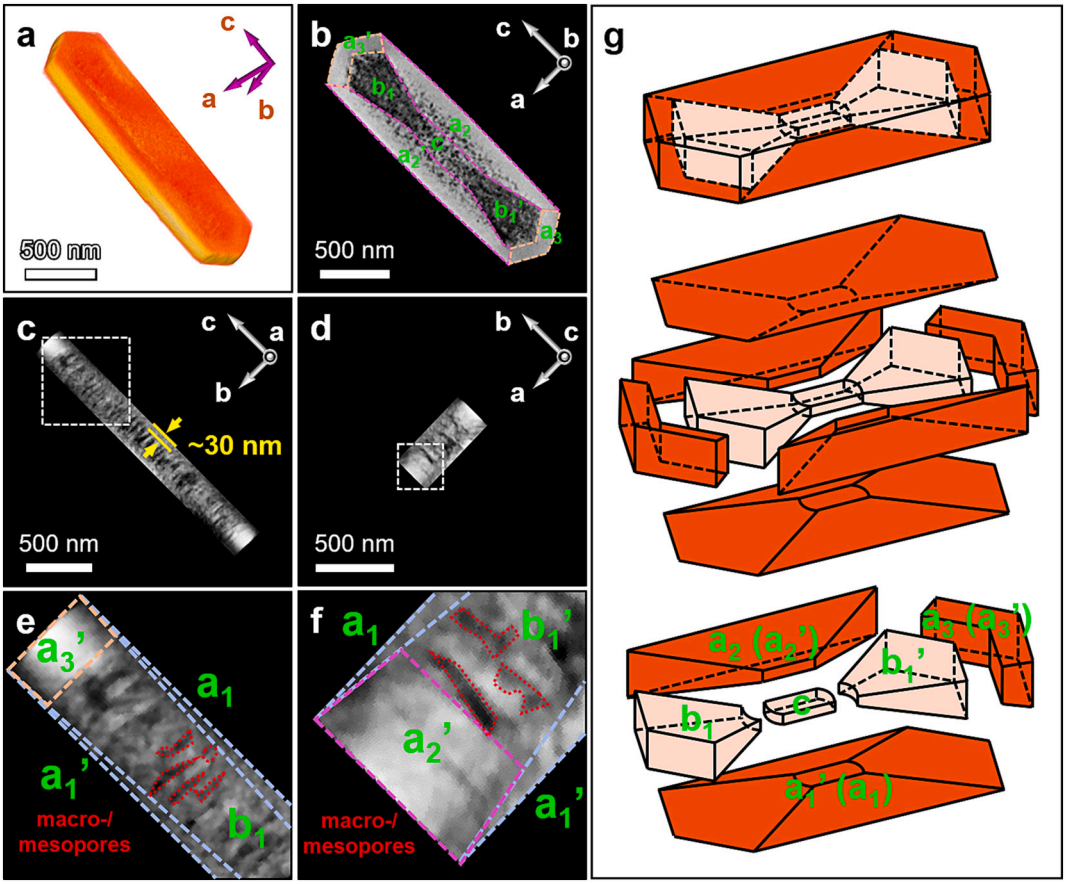

Fig. 2. (a) 3D electron tomographic reconstruction of an individual hourglass-shaped-hollow hierarchical ZSM-5 single crystal. (b–f) HAADF-STEM images of three orthoslices obtained from the 3D reconstruction along (b) *b*-axis, (c, e) *a*-axis and (d, f) *c*-axis, respectively. (g) Schematic illustration of the symmetric volume units of an hourglass-shaped-hollow hierarchical ZSM-5 single crystal, shown in deep orange (slight desilication) and light orange (severe desilication).

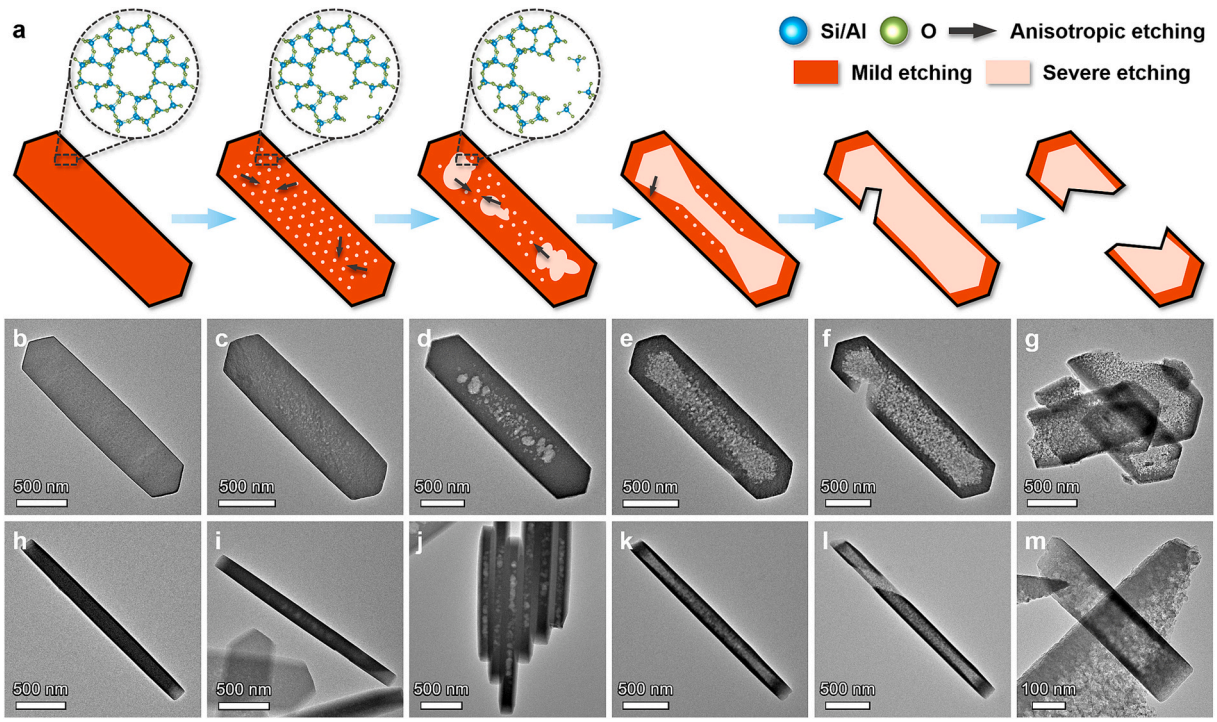

Fig. 3. (a) The alkaline desilication process schematic illustration of an hourglass-shaped-hollow hierarchical ZSM-5 single crystal. (b–m) TEM images of (b, h) AT-0, (c, i) AT-5, (d, j) AT-10, (e, k) AT-15, (f, l) AT-20 and (g, m) AT-25 with different etching times. All the samples are viewed along (b–g) *b*-axis and (h–m) *a*-axis directions.

volume pair consisting of {101} and {10–1} facets with high defects density, and then continue crystallizing to form a complete platelike morphology with aluminum-rich outer surface. The fluorescence microscopy results reported by Roeffaers *et al.* before [37] confirm the above opinions as well. With the aggravation of etching, excessive alkaline treatment caused the trapezoid opening structure perpendicular to the *b*-axis appeared outside the material (Figs. 3f, l and S10), and there is still no obvious alkaline etching trace on the outer surface. It is worth noting that both sides of the etched trapezoidal opening still maintain the same crystal orientation (Fig. S11). When the etching process lasted for 25 min, the hourglass-shaped hierarchically porous ZSM-5 zeolite was completely broken into platelike porous fragments (Figs. 3g, m and S12). The hierarchical zeolite materials in each etching stage maintain perfect single crystal characteristics, uniform element distributions and multi-level pore structures (Figs. S7–S12).

Additionally, in the synthetic system of ZSM-5 zeolite with TPA^+ ions as SDA [38,39] and urea as growth modifier, their organic residues have a great influence on the NaOH desilication process which leading to the formation of hollow hierarchical structure (Figs. S13–S15). On the one hand, the existence of urea and its organic residues further weakens the desilication degree of NaOH; on the other hand, more straight channel openings caused by the adsorption of urea on the specific MFI (010) facet in the hydrothermal process ensure that OH^- diffuses into the zeolite crystal more efficiently. Moreover, the existence of Al zoning is also a non-negligible influential factor in the formation of hollow hierarchical structure [40,41]. The negatively charged Si-O-Al bond is difficult for OH^- to hydrolyze [42,43], as a result OH^- will preferentially attack the Si-O-Si bond in the absence of neighboring Al tetrahedra inside the zeolite crystals. And the quantitative analysis of EDX mapping provides a direct evidence of the relative enrichment of Si element in the internal region of platelike ZSM-5 zeolites (Fig. S16), while Al element are abundantly distributed on the outer surface. Based on the above description, the main factors to form the hollow hourglass-shaped nanosheets include the special shortened *b*-axis crystal morphology, the protective effect of the organic residues of TPA^+ and urea, the Al zoning and the special crystal growth process of the platelike ZSM-5 zeolites.

X-ray diffraction (XRD) patterns illustrate that all etched zeolites exhibit the pure MFI topological phase and high crystallinities (Fig. S17). The Fourier Transform Infrared Spectrometer (FTIR) measurements in the hydroxyl range exhibit an increased intensity of the peak at 3739 cm^{-1}, the disappearance of the absorption at 3724 cm^{-1}, and the first decrease and then increase of the two bands at 3687 and 3602 cm^{-1} (Fig. 4a). Fig. S18 highlights the peak intensity change at 3687 and 3602 cm^{-1}. Specifically, the strong increase of the peak at 3739 cm^{-1} is attributed to the increase of surface silanol groups which resided on the meso-/macropore surface area. The absorption at 3724 cm^{-1} is attributed to the silanol nests which quickly disappeared at the beginning of alkaline etching with NaOH, indicating that the hydroxyl attack is initiated at these defect sites which may mainly distribute in the hourglass region inside the platelike ZSM-5 zeolite (Fig. 3c, i) [37]. And the overall first decrease and then increase intensity of the two bands at 3687 and 3602 cm^{-1} is related to the change of Brønsted acid sites (BASs) density [44,45]. Specifically, when etching time is less than 15 min, the amount of aluminum proportional to the extracted silicon is transformed from Brønsted to Lewis acid sites (LASs) [44]; while in the final etching stage of about 25 min, NaOH would targeted etch LASs and Al species in extra-framework positions and enter the zeolite framework to form BASs through the process of re-alumination [45,46] (Figs. S19, S20 and Tables S1, S2). In addition, after AT-15 was treated with ammonia exchange, the peaks at 3739, 3687 and 3602 cm^{-1} are further enhanced, which indicates the enhanced surface silanol groups and BASs density (Fig. S21).

Further, the ^{29}Si NMR spectra of all etched samples show a mainly intense resonance peak at about −113 ppm (cross-linked Q^4 silica Si $(OSi)_4$ species) and a slightly increased small peak at about −107 ppm (Q^3 silica $Si(OSi)_3(OH)$ and/or $Si(OSi)_3(OAl)$ species) (Fig. 4b), illustrating that the hourglass-shaped-hollow hierarchical ZSM-5 zeolite maintains a good condensation degree with the deepening of etching process. The detailed ^{29}Si NMR peak splitting results of the porous

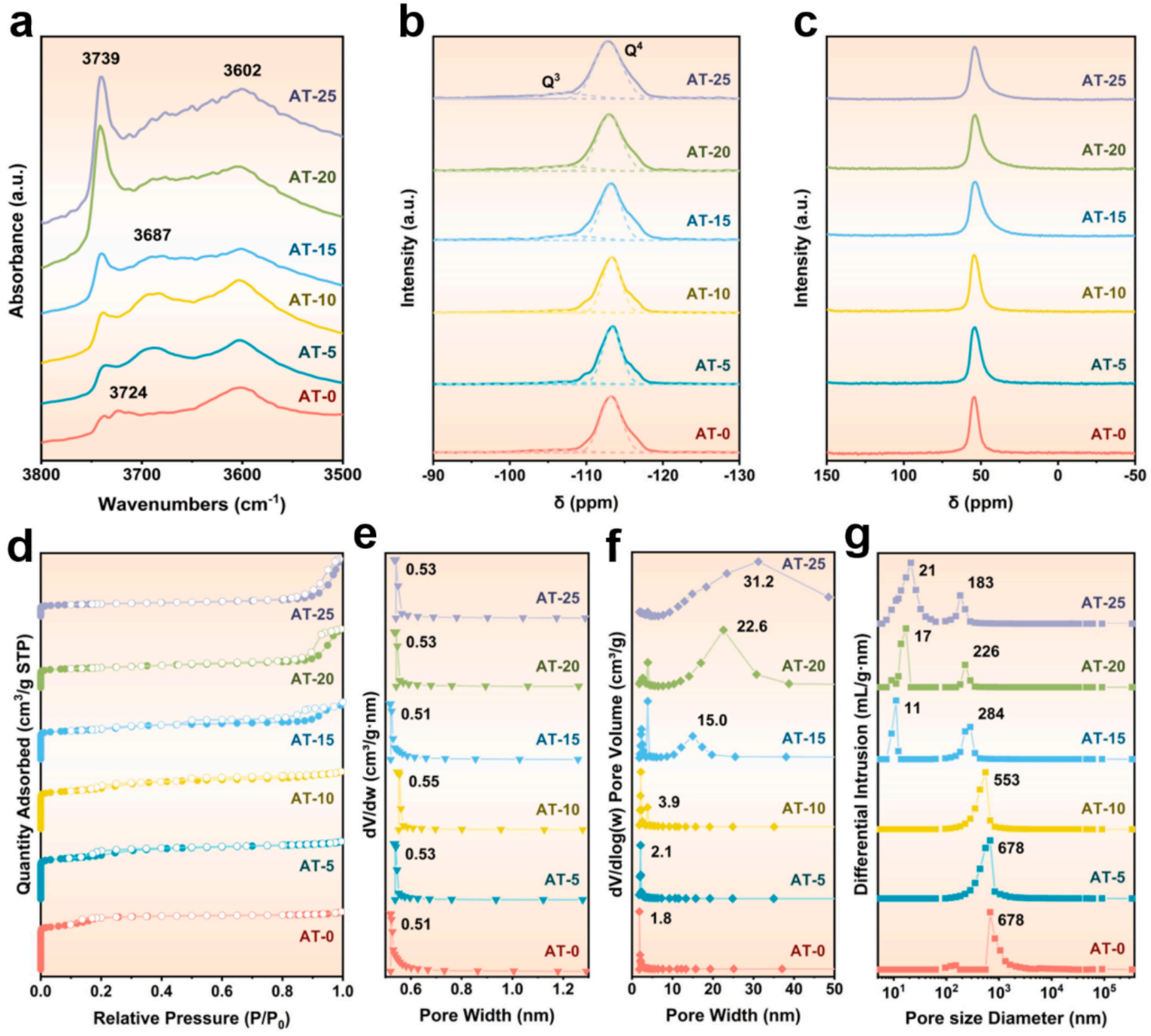

Fig. 4. (a) FTIR spectra in the OH stretching region, (b) ^{29}Si NMR spectra, (c) ^{27}Al NMR spectra, (d) N_2 adsorption-desorption isotherms, the corresponding (e) micropore and (f) mesopore size distributions, and (g) the macropore size distributions adopted from MIP tests of AT-0, AT-5, AT-10, AT-15, AT-20 and AT-25 samples.

zeolites etching for 5 min, 15 min and 25 min shown in Fig. S22 and Table S3 suggest the selective removal of T-site Q^4 silica species during the desilication process, and the relative increase of the defect Q^3 silica species relates to the formation of silanol groups (Fig. 4a). Moreover, a symmetrical signal centered at about 55 ppm has been only shown in the ^{27}Al NMR spectra (Fig. 4c), which indicates that all amorphous aluminum atoms have been successfully incorporated into the zeolite framework and exist in the form of tetrahedral aluminum. The absence of extra-framework aluminum species at 0 ppm can be attributed to the fact that aluminum must initially be taken out of the zeolite and later returned by a re-alumination process during alkaline treatment.

In addition, the N_2 adsorption-desorption isotherms of all etched zeolites exhibit characteristic curves composed by type I ($P/P_0 < 0.01$) and type II ($P/P_0 < 0.95$) isotherms corresponding to the micropores and mesopores, respectively (Fig. 4d). Noted that all zeolites exhibit typical micropore width distribution at about 0.53 nm attributed to the 10-ring channels of MFI topology (Fig. 4e), and mesopore width distribution from 2.1 nm to 31.2 nm attributed to the NaOH etching degree (Fig. 4f). The typical hourglass-shaped-hollow hierarchical ZSM-5 single crystal displays 305 $m^2\ g^{-1}$ BET surface area, 155 $m^2\ g^{-1}$ micropore surface area, 0.08 $cm^3\ g^{-1}$ micropore volume, and 0.26 $cm^3\ g^{-1}$ total pore volume (Table S1). The macropore width distribution adopted by the mercury intrusion porosimetry (MIP) test reveals that the typical macroporous structure (> 50 nm) appeared from 678 nm to 183 nm with the evolution of desilication (Fig. 4g), which can be speculated that the reason of macropore formation changes from the disordered aggregation and accumulation of platelike zeolites to the appearance of intragranular hourglass-shaped structure. Moreover, the hierarchy factor (HF) has been used to describe the porosity of hierarchical porous materials [47], which is calculated through four important textural parameters, as $(V_{micro}/V_{total}) \times (S_{meso}/S_{BET})$. As shown in the final column of Table S1, the HF of samples from AT-0 to AT-15 increases from 0.120

to 0.151, which correlates to the gain in relative mesoporosity (S_{meso}/S_{BET}) exceeding the loss in microporosity (V_{micro}/V_{total}). Generally, materials with more spread hierarchical systems are considered to have improved HF values (HF > 0.15) [47]. However, the HF of samples AT-20 and AT-25 treated with more severely desilication is reduced to 0.084 and 0.054 respectively, which relates to the loss in relative microporosity that has exceeded the gain in relative mesoporosity. Therefore, the hourglass-shaped-hollow hierarchical ZSM-5 single crystal obtained by

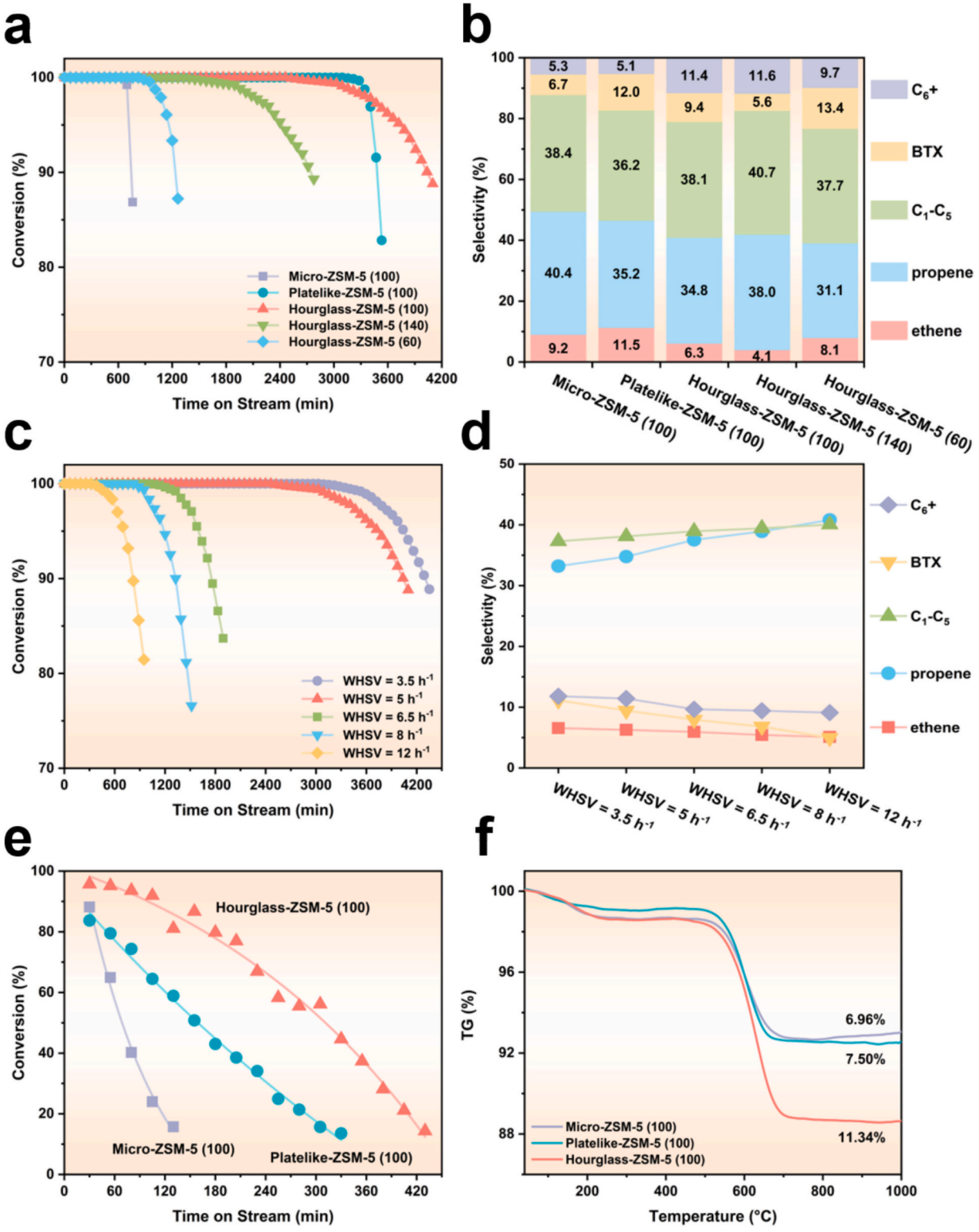

Fig. 5. (a) Methanol conversion with TOS and (b) product distribution when the methanol conversion exceeds 95 % in the reaction system of MTH over micro-ZSM-5 (100), platelike-ZSM-5 (100), hourglass-ZSM-5 (100), hourglass-ZSM-5 (140) and hourglass-ZSM-5 (60) with WHSV = 5 h^{-1}. (c) Methanol conversion with TOS and (d) product distribution over hourglass-ZSM-5 (100) with WHSV = 3.5, 5, 6.5, 8 and 12 h^{-1}. (e) Methanol conversion with WHSV = 70 h^{-1} and (f) TG curves over micro-ZSM-5 (100), platelike-ZSM-5 (100) and hourglass-ZSM-5 (100). Reaction condition: 480 °C.

alkaline desilication simultaneously owns an obvious meso-macroporous structure conducive to diffusion and an accessible microporous structure for efficient catalysis. In short, all NaOH etched hierarchical nanosheets exhibit excellent condensation degrees, increased silanol group concentrations and abundant meso-/macropore distributions (Figs. S23–S39).

The MTH reaction was employed to evaluate the effects of mass diffusion and acid property improvement on the catalytic performance of the obtained hourglass-shaped-hollow hierarchically porous ZSM-5 catalysts. The micro-ZSM-5 (100) (microsized ZSM-5 zeolite with Si/Al as 100), platelike-ZSM-5 (100) (platelike ZSM-5 zeolite with Si/Al as 100) and hourglass-ZSM-5 (x) (hourglass-shaped hierarchical ZSM-5 zeolites with Si/Al as x prepared by alkaline treatment of platelike ZSM-5 zeolites for 15 min, in which x = 100/140/60) have been used as reference catalysts (Figs. S40–S43 and Tables S1, S2). Typically, the MTH reaction was carried out on a fixed-bed reactor under atmospheric pressure at 480 °C. When the weight hourly space velocity (WHSV) of methanol was 5 h^{-1}, the lifetime and product selectivity over all the catalysts are clearly displayed in Figs. 5a, b and S44. Remarkably, the hourglass-ZSM-5 (100) shows the longest catalytic lifetime of about 63.1 h (methanol conversion > 95 %), which is 5.0 times, 3.2 times, 1.5 times and 1.1 times longer than those of micro-ZSM-5 (100), hourglass-ZSM-5 (60), hourglass-ZSM-5 (140) and platelike-ZSM-5 (100), respectively (Table S4). Micro-ZSM-5 (100), platelike-ZSM-5 (100) and hourglass-ZSM-5 (100) possess similar Si/Al and total acidic amount (Table S2). By shortening the *b*-axis thickness, the deactivation of hourglass-ZSM-5 (100) can be effectively slowed down (Fig. 5a), which indicate that shortened diffusion length reduces the probability of coke blocking internal pores [48,49]. Micro-ZSM-5 (100) displays the highest selectivity of propene (40.4 %) affected by the most LASs amount (Fig. 5b and Table S2), since LASs can suppress the conversion of propene to alkanes or aromatics while enhancing the propene desorption rate [50]. As for these with unique hourglass structures, hourglass-ZSM-5 (60) exhibits the shortest catalytic lifetime due to its high-density of BASs that promote the formation of coke precursors which could rapidly deposit on the surface of acid sites (Fig. 5a and Table S2) [51,52]. On the contrary, hourglass-ZSM-5 (140) with low-density of BASs shows high propene/ethene ratio and the reduced BTX selectivity (Figs. 5b and S44f). The detailed product selectivity during the test is shown in Fig. S44a–e. As the reaction proceeds, the propene selectivity of all catalysts gradually decreases, while the selectivity for C_6+ products progressively rises, indicating the transformation of propene into C_6+ products [53]. It is noteworthy that for micro-ZSM-5 (100) and platelike-ZSM-5 (100), the selectivity for propene and C_6+ products undergo abrupt changes once catalyst deactivation begins (Fig. S44a, b), which indicates that hierarchical structure can mitigate the negative effect of catalyst deactivation by providing extra space and enhanced diffusion ability. The superiority of this novel hourglass-ZSM-5 (100) nanosheet performs is attributed to its enhanced diffusivity, anti-coke ability and increased micropore accessibility.

In order to explore the impact of contact time in the MTH reaction performance, a series of catalytic tests on hierarchically hourglass-shaped-hollow ZSM-5 nanosheet (Si/Al = 100) under different WHSV of 3.5, 6.5, 8 and 12 h^{-1} were carried out (Figs. 5c, d and S45). Fig. 5c exhibits that the catalytic lifetime decreases with the increase of WHSV. Specifically, the elevation of WHSV from 3.5 to 5 h^{-1} leads to a slightly decrease of catalyst lifetime, which indicates that the WHSV of 5 h^{-1} was enough to utilize all active sites in catalyst during the lifetime tests. Further increasing the WHSV to 12 h^{-1}, significantly accelerated deactivation is observed and a lifetime of 12.7 h was obtained, indicating that the hierarchically shortened *b*-axis catalyst can achieve decent lifetime under harsh conditions. Fig. 5d displays the product distributions of hourglass-ZSM-5 (100) with varying WHSV = 3.5, 5, 6.5, 8 and 12 h^{-1}. With the increase of WHSV, the propene selectivity increases while the BTX and C_6+ products selectivity decreases. This result illustrates that a high WHSV accelerated the molecular diffusion and lowered the possibility of further adsorption and reaction of intermediates into BTX and C_6+ products. At different space velocities, similar phenomenon of product evolution can be observed (Fig. S45).

To investigate whether such hierarchically shortened *b*-axis ZSM-5 nanosheets are promising for industrial conditions in which a high methanol fraction is used, the MTH reaction with high WHSV of 70 h^{-1} was further performed. In this case, the deactivation behaviors of micro-ZSM-5 (100), platelike-ZSM-5 (100) and hourglass-ZSM-5 (100) were studied, and the corresponding average deactivation rates were calculated (Figs. 5e, S46 and Table S4). In the whole reaction process, all active sites of the catalysts participated in the reaction from the beginning of the MTH tests under the kinetically controlled condition [54,55]. The result shows that hourglass-ZSM-5 (100) performs the lowest deactivation rate (12.20 % h^{-1}), which is 1.15 times and 3.56 times lower than that of platelike-ZSM-5 (100) (14.03 % h^{-1}) and micro-ZSM-5 (100) (43.46 % h^{-1}), respectively. Additionally, the average coke rate of these three catalysts was calculated (Fig. 5f and Table S4). Note that hourglass-ZSM-5 (100) displays an enlarged coke accommodation of 11.34 wt%, which proves that the hierarchically hourglass-shaped-hollow structure possesses the boosting coke capacity and tolerance. Moreover, the average coke rate of hourglass-ZSM-5 (100) is 7.36 mg g^{-1} h^{-1}, which is also 1.06 times and 2.11 times lower than that of platelike-ZSM-5 (100) (7.79 mg g^{-1} h^{-1}) and micro-ZSM-5 (100) (15.52 mg g^{-1} h^{-1}), respectively. The above results strongly support that the introduction of hierarchically shortened *b*-axis structure in MFI zeolite can effectively slow down the deactivation of MTH catalysts, as well as enhanced the diffusivity and coke accommodation capacity.

4. Conclusions

The hierarchically hourglass-shaped-hollow ZSM-5 nanosheet with significantly shortened *b*-axis thickness was successfully designed and synthesized by using facile NaOH desilication strategy. The obtained porous zeolite has a highly interconnected macro-/meso-/micropore structure with the shortest diffusion length along *b*-axis direction less than 30 nm, which exhibits a high HF value, increased accessibility of acid active center and enhanced diffusion performance of straight MFI channels. The abundant *b*-axis straight channel openings and the protective effect of urea and TPA^+ organic residues make it easier for OH^- ions to enter the zeolite and preferentially etch the central area as well as the connected side symmetrical volume pair composed of {101} and {10–1} facets with silicon-rich composition and high defects density. Due to the enhanced mass diffusion and the proper acidity, the hierarchically hourglass-shaped-hollow zeolite ZSM-5 nanosheet with Si/Al = 100 manifests remarkably enhanced catalytic lifetime (63.1 h, WHSV = 5 h^{-1}), which is 5 times longer than that of microsized ZSM-5 zeolite (12.7 h). This work provides a methodological support for the preparation of MFI zeolite with enhanced diffusivity, and provides a theoretical guidance for further understanding the effective relationship between the formation process of hierarchical pores and the intrinsic material synthesis system.

CRediT authorship contribution statement

Zhan Liu: Writing – original draft, Methodology, Data curation. **Ying-Jun He:** Data curation. **Zhi-Yi Hu:** Writing – review & editing, Supervision, Data curation. **Jia-Min Lyu:** Data curation. **Shen Yu:** Data curation. **Yu-Hang Song:** Data curation. **Xiao-Qiang Liao:** Data curation. **Zhi-Wen Yin:** Data curation. **Ming-Hui Sun:** Data curation. **Yu-Chun Zhi:** Supervision, Data curation. **Li-Hua Chen:** Writing – review & editing, Supervision, Project administration. **Bao-Lian Su:** Supervision, Project administration.

Declaration of competing interest

The authors declare that they have no known competing financial

interests or personal relationships that could have appeared to influence the work reported in this paper.

Acknowledgements

This work is financially supported by National Key Research and Development Program of China (2022YFB3504000), National Natural Science Foundation of China (22293022, U20A20122, 52103285, U22B6011), Program of Introducing Talents of Discipline to Universities-Plan 111 (Grant No. B20002) from the Ministry of Science and Technology and the Ministry of Education of China, Natural Science Foundation of Hubei Province (2023AFB605, 2025AFB033), and Dawning Program of Wuhan (2023020201020306). This research was also supported by the European Commission Interreg V France-Wallonie-Vlaanderen project "DepollutAir", the Program Win2Wal (TCHARBONACTIF: 2110120), Wallonia Region of Belgium and the National Key Research and Development Program Intergovernmental Technological Innovation Special Cooperation Project Wallonia-Brussels/China (MOST) (SUB/2021/IND493971/524448). B.-L. Su acknowledges a Clare Hall Life Membership, University of Cambridge. L.-H. Chen acknowledges Hubei Provincial Department of Education for the "Chutian Scholar" program.

Appendix A. Supplementary data

Supplementary data to this article can be found online at https://doi.org/10.1016/j.cej.2025.167120.

Data availability

Data will be made available on request.

References

[1] U. Olsbye, S. Svelle, M. Bjørgen, P. Beato, T.V.W. Janssens, F. Joensen, S. Bordiga, K.P. Lillerud, Conversion of methanol to hydrocarbons: how zeolite cavity and pore size controls product selectivity, Angew. Chem. Int. Ed. Engl. 51 (24) (2012) 5810–5831.
[2] S. Teketel, W. Skistad, S. Benard, U. Olsbye, K.P. Lillerud, P. Beato, S. Svelle, Shape selectivity in the conversion of methanol to hydrocarbons: the catalytic performance of one-dimensional 10-ring zeolites: ZSM-22, ZSM-23, ZSM-48, and EU-1, ACS Catal. 2 (1) (2011) 26–37.
[3] L. Qi, Y. Wei, L. Xu, Z. Liu, Reaction behaviors and kinetics during induction period of methanol conversion on HZSM-5 zeolite, ACS Catal. 5 (7) (2015) 3973–3982.
[4] I. Yarulina, A.D. Chowdhury, F. Meirer, B.M. Weckhuysen, J. Gascon, Recent trends and fundamental insights in the methanol-to-hydrocarbons process, Nat. Catal. 1 (6) (2018) 398–411.
[5] U. Olsbye, S. Svelle, K.P. Lillerud, Z.H. Wei, Y.Y. Chen, J.F. Li, J.G. Wang, W.B. Fan, The formation and degradation of active species during methanol conversion over protonated zeotype catalysts, Chem. Soc. Rev. 44 (20) (2015) 7155–7176.
[6] A.D. Chowdhury, K. Houben, G.T. Whiting, M. Mokhtar, A.M. Asiri, S.A. Al-Thabaiti, S.N. Basahel, M. Baldus, B.M. Weckhuysen, Initial carbon-carbon bond formation during the early stages of the methanol-to-olefin process proven by zeolite-trapped acetate and methyl acetate, Angew. Chem. Int. Ed. Engl. 55 (51) (2016) 15840–15845.
[7] M. Yang, D. Fan, Y. Wei, P. Tian, Z. Liu, Recent progress in methanol-to-olefins (MTO) catalysts, Adv. Mater. 31 (50) (2019) e1902181.
[8] P. Tian, Y. Wei, M. Ye, Z. Liu, Methanol to olefins (MTO): from fundamentals to commercialization, ACS Catal. 5 (3) (2015) 1922–1938.
[9] N. Wang, W. Qian, K. Shen, C. Su, F. Wei, Bayberry-like ZnO/MFI zeolite as high performance methanol-to-aromatics catalyst, Chem. Commun. 52 (10) (2016) 2011–2014.
[10] C.-Y. Hsieh, Y.-Y. Chen, Y.-C. Lin, Ga-substituted nanoscale HZSM-5 in methanol aromatization: the cooperative action of the Brønsted acid and the extra-framework Ga species, Ind. Eng. Chem. Res. 57 (23) (2018) 7742–7751.
[11] T. Li, T. Shoinkhorova, J. Gascon, J. Ruiz-Martínez, Aromatics production via methanol-mediated transformation routes, ACS Catal. 11 (13) (2021) 7780–7819.
[12] Z. Wan, W. Wu, G. Li, C. Wang, H. Yang, D. Zhang, Effect of SiO_2/Al_2O_3 ratio on the performance of nanocrystal ZSM-5 zeolite catalysts in methanol to gasoline conversion, Appl. Catal. A-Gen. 523 (2016) 312–320.
[13] A. Galadima, O. Muraza, From synthesis gas production to methanol synthesis and potential upgrade to gasoline range hydrocarbons: a review, J. Nat. Gas Sci. Eng. 25 (2015) 303–316.
[14] S. Fathi, M. Sohrabi, C. Falamaki, Improvement of HZSM-5 performance by alkaline treatments: comparative catalytic study in the MTG reactions, Fuel 116 (2014) 529–537.
[15] G.T. Kokotailo, S.L. Lawton, D.H. Olson, Structure of synthetic zeolite ZSM-5, Nature 272 (1978) 437–438.
[16] S.M. Csicsery, Shape-selective catalysis in zeolites, Zeolites 4 (1984) 202–213.
[17] Z. Wang, L.A. O'Dell, X. Zeng, C. Liu, S. Zhao, W. Zhang, M. Gaborieau, Y. Jiang, J. Huang, Insight into three-coordinate aluminum species on ethanol-to-olefin conversion over ZSM-5 zeolites, Angew. Chem. Int. Ed. Engl. 58 (50) (2019) 18061–18068.
[18] S. Zhao, W.D. Wang, L. Wang, W. Schwieger, W. Wang, J. Huang, Tuning hierarchical ZSM-5 zeolite for both gas- and liquid-phase biorefining, ACS Catal. 10 (2) (2019) 1185–1194.
[19] M. Hartmann, A.G. Machoke, W. Schwieger, Catalytic test reactions for the evaluation of hierarchical zeolites, Chem. Soc. Rev. 45 (12) (2016) 3313–3330.
[20] J. Huangfu, D. Mao, X. Zhai, Q. Guo, Remarkably enhanced stability of HZSM-5 zeolite co-modified with alkaline and phosphorous for the selective conversion of bio-ethanol to propylene, Appl. Catal. A-Gen. 520 (2016) 99–104.
[21] D. Fu, J.J.E. Maris, K. Stanciakova, N. Nikolopoulos, O. van der Heijden, L.D. B. Mandemaker, M.E. Siemons, D. Salas Pastene, L.C. Kapitein, F.T. Rabouw, F. Meirer, B.M. Weckhuysen, Unravelling channel structure-diffusivity relationships in zeolite ZSM-5 at the single-molecule level, Angew. Chem. Int. Ed. Engl. 61 (5) (2022) e202114388.
[22] J. Duan, W. Chen, C. Wang, L. Wang, Z. Liu, X. Yi, W. Fang, H. Wang, H. Wei, S. Xu, Y. Yang, Q. Yang, Z. Bao, Z. Zhang, Q. Ren, H. Zhou, X. Qin, A. Zheng, F.S. Xiao, Coking-resistant polyethylene upcycling modulated by zeolite micropore diffusion, J. Am. Chem. Soc. 144 (31) (2022) 14269–14277.
[23] J. Zhang, A. Zhou, K. Gawande, G. Li, S. Shang, C. Dai, W. Fan, Y. Han, C. Song, L. Ren, A. Zhang, X. Guo, *b*-Axis-oriented ZSM-5 nanosheets for efficient alkylation of benzene with methanol: synergy of acid sites and diffusion, ACS Catal. 13 (6) (2023) 3794–3805.
[24] J. Zhang, L. Ren, A. Zhang, X. Guo, C. Song, MFI Nanosheets: a rising star in zeolite materials, Mater. Chem. Front. 8 (3) (2024) 595–602.
[25] S. Mintova, J. Grand, V. Valtchev, Nanosized zeolites: quo Vadis? C. R. Chim. 19 (1–2) (2016) 183–191.
[26] J. Pérez-Ramírez, C.H. Christensen, K. Egeblad, C.H. Christensen, J.C. Groen, Hierarchical zeolites: enhanced utilisation of microporous crystals in catalysis by advances in materials design, Chem. Soc. Rev. 37 (11) (2008) 2530–2542.
[27] L.-H. Chen, M.-H. Sun, Z. Wang, W. Yang, Z. Xie, B.-L. Su, Hierarchically structured zeolites: from design to application, Chem. Rev. 120 (20) (2020) 11194–11294.
[28] H. Dai, Y. Shen, T. Yang, C. Lee, D. Fu, A. Agarwal, T.T. Le, M. Tsapatsis, J. C. Palmer, B.M. Weckhuysen, P.J. Dauenhauer, X. Zou, J.D. Rimer, Finned zeolite catalysts, Nat. Mater. 19 (10) (2020) 1074–1080.
[29] M.-H. Sun, J. Zhou, Z.-Y. Hu, L.-H. Chen, L.-Y. Li, Y.-D. Wang, Z.-K. Xie, S. Turner, G. Van Tendeloo, T. Hasan, B.-L. Su, Hierarchical zeolite single-crystal reactor for excellent catalytic efficiency, Matter 3 (4) (2020) 1226–1245.
[30] Z. Liu, J.-M. Lyu, C.-M. Guo, Z.-Y. Hu, M.-H. Sun, L.-H. Chen, B.-L. Su, Tunable acidity and porosity for optimizing liquid-phase catalytic efficiency utilizing hierarchical zeolite ZSM-5 single crystal reactor, Micropor. Mesopor. Mater. 387 (2025) 113509.
[31] M. Choi, K. Na, J. Kim, Y. Sakamoto, O. Terasaki, R. Ryoo, Stable single-unit-cell nanosheets of zeolite MFI as active and long-lived catalysts, Nature 461 (7261) (2009) 246–249.
[32] L. Tan, N. Jiao, X. Bai, H. Wang, J. Wang, H. Wang, X. Zhang, Methods for preparing hierarchical zeolites by chemical etching and their catalytic applications: a review, Eur. J. Inorg. Chem. 26 (24) (2023) e202300314.
[33] F. Meng, X. Wang, S. Wang, Y. Wang, Fluoride-treated HZSM-5 as a highly stable catalyst for the reaction of methanol to gasoline, Catal. Today 298 (2017) 226–233.
[34] C. Mei, P. Wen, Z. Liu, H. Liu, Y. Wang, W. Yang, Z. Xie, W. Hua, Z. Gao, Selective production of propylene from methanol: mesoporosity development in high silica HZSM-5, J. Catal. 258 (1) (2008) 243–249.
[35] T. Zhou, D. Zhang, Y. Liu, Y. Sun, T. Ji, S. Huang, Y. Liu, Construction of monodispersed single-crystalline hierarchical ZSM-5 nanosheets via anisotropic etching, J. Energy Chem. 72 (2022) 516–521.
[36] Y. Liu, W. Qiang, T. Ji, M. Zhang, M. Li, J. Lu, Y. Liu, Uniform hierarchical MFI nanosheets prepared via anisotropic etching for solution-based sub-100-nm-thick oriented MFI layer fabrication, Sci. Adv. 6 (2020) eaay5993.
[37] M.B.J. Roeffaers, R. Ameloot, M. Baruah, H. Uji-i, M. Bulut, G.D. Cremer, U. Müller, P.A. Jacobs, J. Hofkens, B.F. Sels, D.E.D. Vos, Morphology of large ZSM-5 crystals unraveled by fluorescence microscopy, J. Am. Chem. Soc. 130 (2008) 5763–5772.
[38] L. Brabec, M. Kocirik, Silicalite-1 crystals etched with hydrofluoric acid dissolved in water or acetone, J. Phys. Chem. C 114 (2010) 13685–13694.
[39] J. Pérez-Ramírez, S. Abelló, A. Bonilla, J.C. Groen, Tailored mesoporosity development in zeolite crystals by partial detemplation and desilication, Adv. Funct. Mater. 19 (1) (2008) 164–172.
[40] R.v. Ballmoos, W.M. Meier, Zoned aluminium distributionin synthetic zeolite ZSM-5, Nature 298 (1981) 782–783.
[41] C.G. Johan, B. Torkel, Z. Ulrike, M.P.-v.D. Anne, P.d.J. Krijn, A.M. Jacob, J. Pérez-Ramírez, Creation of hollow zeolite architectures by controlled desilication of Al-zoned ZSM-5 crystals, J. Am. Chem. Soc. 127 (2005) 10792–10793.
[42] J.C. Groen, J.A. Moulijn, J. Pérez-Ramírez, Desilication: on the controlled generation of mesoporosity in MFI zeolites, J. Mater. Chem. 16 (22) (2006) 2121–2131.
[43] Č. Ankica, S. Boris, Š. Ivan, T. Antun, A. Rosario, C. Fortunato, N. Alfonso, Dissolution of high-silica zeolites in alkaline solutions II. Dissolution of 'activated' silicalite-1 and ZSM-5 with different aluminum content, Micropor. Mater. 8 (3–4) (1997) 159–169.

[44] D. Verboekend, J.C. Groen, J. Pérez-Ramírez, Interplay of properties and functions upon introduction of mesoporosity in ITQ-4 zeolite, Adv. Funct. Mater. 20 (9) (2010) 1441–1450.
[45] J.C. Groen, L.A.A. Peffer, J.A. Moulijn, J. Pérez-Ramírez, Mechanism of hierarchical porosity development in MFI zeolites by desilication: the role of aluminium as a pore-directing agent, Chem. A Eur. J. 11 (17) (2005) 4983–4994.
[46] J.C. Groen, J.C. Jansen, J.A. Moulijn, J. Pérez-Ramírez, Optimal aluminum-assisted mesoporosity development in MFI zeolites by desilication, J. Phys. Chem. B 108 (2004) 13062–13065.
[47] J. Pérez-Ramírez, D. Verboekend, A. Bonilla, S. Abelló, Zeolite catalysts with tunable hierarchy factor by pore-growth moderators, Adv. Funct. Mater. 19 (24) (2009) 3972–3979.
[48] N. Wang, W. Sun, Y. Hou, B. Ge, L. Hu, J. Nie, W. Qian, F. Wei, Crystal-plane effects of MFI zeolite in catalytic conversion of methanol to hydrocarbons, J. Catal. 360 (2018) 89–96.
[49] N. Kalantari, M.F. Bekheet, P.D.K. Nezhad, J.O. Back, A. Farzi, S. Penner, N. Delibas, S. Schwarz, J. Bernardi, D. Salari, A. Niaei, Effect of chromium and boron incorporation methods on structural and catalytic properties of hierarchical ZSM-5 in the methanol-to-propylene process, J. Ind. Eng. Chem. 111 (2022) 168–182.
[50] S. Han, D. Zhao, T. Otroshchenko, H. Lund, U. Bentrup, V.A. Kondratenko, N. Rockstroh, S. Bartling, D.E. Doronkin, J.-D. Grunwaldt, U. Rodemerck, D. Linke, M. Gao, G. Jiang, E.V. Kondratenko, Elucidating the nature of active sites and fundamentals for their creation in Zn-containing ZrO_2-based catalysts for nonoxidative propane dehydrogenation, ACS Catal. 10 (2020) 8933–8949.
[51] X. Wu, Y. Wei, Z. Liu, Dynamic catalytic mechanism of the methanol-to-hydrocarbons reaction over zeolites, Acc. Chem. Res. 56 (14) (2023) 2001–2014.
[52] R. Liu, X. Shao, C. Wang, W. Dai, N. Guan, Reaction mechanism of methanol-to-hydrocarbons conversion: fundamental and application, Chin. J. Catal. 47 (2023) 67–92.
[53] L. Lin, M. Fan, A.M. Sheveleva, X. Han, Z. Tang, J.H. Carter, I. da Silva, C.M. A. Parlett, F. Tuna, E.J.L. McInnes, G. Sastre, S. Rudić, H. Cavaye, S.F. Parker, Y. Cheng, L.L. Daemen, A.J. Ramirez-Cuesta, M.P. Attfield, Y. Liu, C.C. Tang, B. Han, S. Yang, Control of zeolite microenvironment for propene synthesis from methanol, Nat. Commun. 12 (2021) 822.
[54] Q. Xiao, T.U. Connell, J.J. Cadusch, A. Roberts, A.S.R. Chesman, D.E. Gómez, Hot-carrier organic synthesis via the near-perfect absorption of light, ACS Catal. 8 (2018) 10331–10339.
[55] S.L. Scott, A matter of life(time) and death, ACS Catal. 8 (2018) 8597–8599.